Enhanced angiogenesis and increased cardiac perfusion after myocardial infarction in protein tyrosine phosphatase 1B-deficient mice

Marie Besnier,[*,†] Ariane Galaup,[‡] Lionel Nicol,[*,†] Jean-Paul Henry,[*,†] David Coquerel,[*,†] Alexandre Gueret,[*,†] Paul Mulder,[*,†] Ebba Brakenhielm,[*,†] Christian Thuillez,[*,†] Stéphane Germain,[‡] Vincent Richard,[*,†] and Antoine Ouvrard-Pascaud[*,†,1]

*Institut National de la Santé et de la Recherche Médicale (INSERM) U1096, Rouen, France; [†]Institute of Research and Innovations in Biomedicine (IRIB), University of Rouen, Rouen, France; and [‡]INSERM U1050, Center for Interdisciplinary Research in Biology, Collège de France, Paris, France

ABSTRACT **The protein tyrosine phosphatase 1B (PTP1B) modulates tyrosine kinase receptors, among which is the vascular endothelial growth factor receptor type 2 (VEGFR2), a key component of angiogenesis. Because PTP1B deficiency in mice improves left ventricular (LV) function 2 mo after myocardial infarction (MI), we hypothesized that enhanced angiogenesis early after MI *via* activated VEGFR2 contributes to this improvement. At 3 d after MI, capillary density was increased at the infarct border of *PTP1B*$^{-/-}$ mice [+7±2% *vs.* wild-type (WT), $P = 0.05$]. This was associated with increased extracellular signal-regulated kinase 2 phosphorylation and VEGFR2 activation (*i.e.*, phosphorylated-Src/Src/VEGFR2 and dissociation of endothelial VEGFR2/VE-cadherin), together with higher infiltration of proangiogenic M2 macrophages within unchanged overall infiltration. *In vitro*, we showed that PTP1B inhibition or silencing using RNA interference increased VEGF-induced migration and proliferation of mouse heart microvascular endothelial cells as well as fibroblast growth factor (FGF)-induced proliferation of rat aortic smooth muscle cells. At 8 d after MI in *PTP1B*$^{-/-}$ mice, increased LV capillary density (+21±3% *vs.* WT; $P<0.05$) and an increased number of small diameter arteries (15–50 μm) were likely to participate in increased LV perfusion assessed by magnetic resonance imaging and improved LV compliance, indicating reduced diastolic dysfunction. In conclusion, PTP1B deficiency reduces MI-induced heart failure promptly after ischemia by enhancing angiogenesis, myocardial perfusion, and diastolic function.—Besnier, M., Galaup, A., Nicol, L., Henry, J.-P, Coquerel, D., Gueret, A., Mulder, P., Brakenhielm, E., Thuillez, C., Germain, S., Richard, V., Ouvrard-Pascaud, A. Enhanced angiogenesis and increased cardiac perfusion after myocardial infarction in protein tyrosine phosphatase 1B-deficient mice. *FASEB J.* 28, 3351–3361 (2014). www.fasebj.org**

Key Words: vascular growth · growth factors · cytokines

Chronic heart failure (CHF) after myocardial infarction (MI) is a major cause of death that is steadily increasing worldwide. Despite standardized therapy, the prognosis remains poor in patients who commonly display left ventricular (LV) dysfunction. A promising approach consists of stimulating angiogenesis/arteriogenesis and/or preserving a functional cardiac vascular network after MI, which may help to improve cardiac perfusion and function (1, 2).

Several growth factors, such as vascular endothelial growth factor (VEGF), platelet-derived growth factor (PDGF), fibroblast growth factor (FGF), and hepato-

Abbreviations: αSMA, α-smooth muscle actin; CHF, chronic heart failure; eNOS, endothelial nitric oxide synthase; ERK-1/2, extracellular signal-regulated kinase 1/2; FCS, fetal calf serum; FGF, fibroblast growth factor; GAPDH, glyceraldehyde-3-phosphate dehydrogenase; HGF, hepatocyte growth factor; HMEC, heart microvascular endothelial cell; HUVEC, human umbilical vein endothelial cell; LV, left ventricular; LVEDPVR, left ventricular end-diastolic pressure-volume relation; LVESPVR, left ventricular end-systolic pressure-volume relation; MI, myocardial infarction; MRI, magnetic resonance imaging; NO, nitric oxide; PDGF, platelet derived growth factor; PECAM-1, platelet and endothelial cell adhesion molecule 1; PFA, paraformaldehyde; PI3K, phosphatidylinositol 3-kinase; PTP1B, protein tyrosine phosphatase 1B; rh, recombinant human; RTK, receptor tyrosine kinase; SA, streptavidin; shRNA, short hairpin RNA; siRNA, small interfering RNA; SNAP, *S*-nitroso-*N*-acetyl-DL-penicillamine; VE-cadherin, vascular endothelial cadherin; VEGF, vascular endothelial growth factor; VSMC, vascular smooth muscle cell; WT, wild type

[1] Correspondence: Inserm U1096, UFR Médecine Pharmacie, 22 Bd Gambetta, 76183 Rouen Cedex, France. E-mail: antoine.ouvrard-pascaud@univ-rouen.fr

doi: 10.1096/fj.13-245753

This article includes supplemental data. Please visit *http://www.fasebj.org* to obtain this information.

cyte growth factor (HGF), and numerous cell types, including endothelial cells, vascular smooth muscle cells (VSMCs), and immune cells, such as monocytes/macrophages, are implicated in angiogenesis. Growth factors bind to different types of receptor tyrosine kinases (RTKs), which are activated by tyrosine (Y) phosphorylation and subjected to negative regulation by phosphatases.

The protein tyrosine phosphatase 1B (PTP1B) was first described as a modulator of the β-subunit of insulin RTK, leading to reduced insulin sensitivity (3), and has also been implicated in the regulation of leptin sensitivity (4). Moreover, PTP1B suppresses/inhibits signaling pathways downstream of the VEGF, PDGF, FGF, and HGF receptors (5–8), suggesting that blocking of PTP1B might stimulate angiogenesis induced by these growth factors. In fact, in cultured VSMCs, overexpression of PTP1B decreased PDGF-induced cell motility associated with decreased tyrosine phosphorylation of PDGF receptor-β (7). Conversely, suppression of PTP1B expression by small interfering RNA (siRNA) increased phosphorylation of focal adhesion proteins (paxilline, p130cas, and focal adhesion kinase; ref. 9).

Concerning CHF, we recently demonstrated that long-term administration of a selective PTP1B inhibitor or gene invalidation in *PTP1B*$^{-/-}$ mice not only restored endothelial function but also improved cardiac remodeling and function at 1 and 2 mo post-MI, suggesting that this phosphatase may constitute a promising new treatment for CHF (10); however, this previous study did not assess any possible changes in angiogenesis/arteriogenesis or cardiac perfusion. We thus now hypothesize that increased cardiac angiogenesis/arteriogenesis, possibly leading to improved cardiac perfusion, could be one of the mechanisms behind these previously reported beneficial cardiac effects.

In this study, we performed an *in vitro* study in cultured vascular cells to assess the effect of pharmacological inhibition or transcriptional blockage (siRNA) of PTP1B on processes involved in angiogenesis. Then, we evaluated the effects of PTP1B gene invalidation (using *PT1P1B*$^{-/-}$ mice) on myocardial angiogenesis/arteriogenesis after MI as an early event supporting cardiac perfusion and function.

MATERIALS AND METHODS

Cell culture, migration, proliferation, and apoptosis

Mouse heart microvascular endothelial cells (HMECs; ref. 11) were a gift from Dr. M. Presta (Università di Brescia, Brescia, Italy). Cells were transduced with a lentivirus containing short hairpin RNA (shRNA) against PTP1B (CCGGCGGATTAAATTGCACCAGGAACTCGAGTTCCTGGTGCAATTTAATCCGTTTTT) and a puromycin resistance gene that allowed selection of the HMEC Sh1 subclone (2 μg/ml puromycin). Cells were cultivated on fibronectin (2.5 μg/ml)-coated plates in Dulbecco's modified Eagle's medium (Life Technologies, Inc., Invitrogen, UK) containing 10% fetal calf serum (FCS), 50 U/ml penicillin, and 50 μg/ml streptomycin at 37°C and 5% CO_2 in a humidified atmosphere. Rat aortic VSMCs in primary culture were purchased from Lonza France SARL (Levallois, France) and grown as recommended by the manufacturer.

Migration was assessed in cells starved overnight in 1% FCS with or without the PTP1B inhibitor AS279 at 1 μM (Merck-Serono Pharmaceutical Research Institute, Darmstadt, Germany; ref. 12). One hour before trypsin, starvation medium was replaced by serum-free medium containing 0.25% bovine serum albumin. Cells were seeded in Boyden chambers at a density of 10^4 cells/upper well, separated from lower wells by a 8-μm microporated membrane (NeuroProbe Inc., Gaithersburg, MD, USA) coated with 16 μg/ml fibronectin (BD, Franklin Lakes, NJ, USA). Lower wells contained 50 ng/ml recombinant human (rh) VEGF-A (16-aa dimer; R&D Systems, Inc., Minneapolis, MN, USA) or 25 ng/ml rhPDGF-BB (109-aa dimer; R&D Systems) with or without 1 μM AS279. After 6 h of incubation, cells migrating across the membrane were fixed in methanol and stained with hematoxylin. With use of light microscopy, 3 images were taken at ×40 for each well, and cells were counted. Six replicates were made per condition, and experiments were repeated 3 times. Results are given as mean numbers of cells per field.

Proliferation was assessed in HMECs and VSMCs starved in 1% FCS for 24 h with or without 1 μM AS279 for 4 h. After trypsinization, cells were seeded at 10^4 cells/well in 24-well plates. After attachment, medium was replaced by growth medium in the absence or presence of 25 ng/ml rhVEGF-A or 25 ng/ml rhFGF-2 (157-aa monomer; R&D Systems). Proliferation was measured after 48 h using a Coulter counter for HMECs or a WST-1 assay for VSMCs, according to the manufacturer's instructions (Roche Molecular Biochemicals, Mannheim, Germany).

Apoptosis was assessed in HMECs and Sh1 cells seeded at 10^4 cells/well in 96-well plates and starved after attachment in 2% FCS overnight before the addition of 1 μM staurosporine for 6 h to induce apoptosis in the absence or the presence of 1 μM AS279 added 1 h before staurosporine. Caspase-3 activity was evaluated as a luminescent signal read on a Mithras Microplate Reader LB940 (Berthold Technologies, Thoiry, France) using a caspase-3/7 glow kit (Promega, Madison, WI, USA), according to manufacturer's instructions.

RT-PCR

HMECs and Sh1 cells were lysed (4 M guanidine thiocyanate; 0.75 M sodium citrate, pH 7; 10% sarcosyl; and 0.7% mercaptoethanol) and snap-frozen at −80°C. RNA was extracted using acid phenol-chloroform. RNA quantity and purity were assessed with an ND 1000 Spectrophotometer (NanoDrop Technologies, Wilmington, DE, USA). Then 1 μg of RNA was used for reverse transcription with 2.5 μg of hexameric random probes [100 pmol/μl oligonucleotide pd(N)6], 10 mM dNTP, 40 U of RNaseOUT, and 200 U of RT (Moloney murine leukemia virus reverse transcriptase; Life Technologies) for 1 h at 37°C. Real-time PCR was performed using a commercial mix containing *Taq*DNA polymerase, SYBR Green I, and $MgCl_2$ (FastStart DNA Master SYBR Green I kit; Roche Molecular Biochemicals) and a LightCycler (Roche Molecular Biochemicals). Primers were as follows: murine PTP1B, 5′-TCATCCAGACTGCCGACCA-3′ (sense) and 5′-ATGATGAACTTGGCGCCCTCG-3′ (antisense); and murine 18S, 5′-GTGGAGCGATTTGTCTGGTT-3′ (sense) and 5′-CGCTGAGCCAGTCAGTGTAG-3′ (antisense). Data were analyzed using LightCycler software.

Animals

The *PTP1B*$^{-/-}$ mouse line was obtained from Dr. Michel L. Tremblay (Goodman Cancer Centre, McGill University, Montreal, QC, Canada). *PTP1B*$^{-/-}$ mice and wild-type (WT) littermates were obtained by crossing BALB/c *PTP1B*$^{+/-}$ mice. The genotype was determined by PCR of tail genomic DNA. We used 10- to 12-week-old *PTP1B*$^{-/-}$ and WT male mice. Animal experiments were performed in accordance with the U.S. National Institutes of Health guidelines, the European Communities Council Directives (86/609/EEC), and French National legislation (ethical approval no. B76-114). The investigation conforms to Directive 2010/63/EU of the European Parliament. The animal protocol was approved by the Normandy ethics review board.

MI

MI was induced by left coronary artery ligation in mice as described previously (10, 12). At 1, 3, and 8 d and 3 mo after MI, mice were euthanized by cervical disruption. Hearts were rapidly excised and arrested in ice-cold saturated KCl buffer. The left ventricle was dissected before being snap-frozen in liquid nitrogen for Western blot analyses, embedded in Tissue-Tek (Sakura Finetek USA, Torrance, CA, USA) for immunohistological analyses, or fixed in Bouin's solution or in formaldehyde for histochemical analysis. For assessment of the diameter of α-smooth muscle actin (αSMA)-positive arteries, anesthetized animals were perfused through the LV cavity with 3 ml of heparin (10 U/ml) followed by 10 ml of preheated 2% paraformaldehyde (PFA). Left ventricles were then dissected and incubated successively in baths of 4% PFA (1 h), 10% sucrose (1 h), 20% sucrose (1 h), and 30% sucrose (overnight) before being snap-frozen in liquid nitrogen and stored at −80°C.

Histochemistry

Infarct size and LV fibrosis were assessed in 6- to 10-μm-thick heart sections fixed in Bouin's solution and stained with sirius red as described previously (13) for 3 mo post-MI analysis or stained by Masson's trichrome protocol for 3 d analysis. We used 2 different staining protocols because collagen staining with sirius red is highly relevant in healed infarcts essentially composed of scar tissue; however, it is unusable in the context of early infarcts that have not yet been replaced by scar tissue and by collagen. Thus, we chose Masson's trichrome at 3 d, before this stain effectively detects necrotic cell. For infarct size, 5–7 serial sections obtained every 600 μm, starting at the level of the ligation, were stained and photographed under a light microscope (Carl Zeiss GmbH, Jena, Germany) at ×1.25 view. Image Pro-Plus 6.3 software (MediaCybernetics, Rockville, MD, USA) was used for image analysis. MI size was calculated as total infarction perimeter/(epicardial LV perimeter + endocardial LV perimeter) × 100 at 3 mo post-MI; however, at 3 d post-MI, the percentage of LV infarcted area was measured because at this early time point, the infarct scar has not completely formed. LV fibrosis was assessed at 3 mo post-MI as described previously (13).

For assessment of hemorrhage, the left ventricle was fixed in 4% formaldehyde and embedded in paraffin. Then 4-μm sections were stained using Masson's trichrome protocol.

Immunohistochemistry

Heart cryosections (6–10 μm) were fixed in acetone and stained according to standard protocols using biotinylated rat anti-mouse platelet and endothelial cell adhesion molecule-1 (PECAM-1; 1:100; BD), mouse anti-human αSMA-fluorescein isothiocyanate (1:200; Sigma-Aldrich, St. Louis, MO, USA), rabbit anti-human Ki67 (1:500; Novocastra Laboratories, Newcastle, UK), rat anti-mouse F4/80 (1:200; Serotec, Oxford, UK), rat anti-mouse CD45 (1:10; BD), rabbit anti-mouse MRC-1/CD206 (1:200; Santa Cruz Biotechnology), rabbit anti-mouse cleaved caspase-3 (1:300; Cell Signaling Technology, Danvers, MA, USA), and wheat germ agglutinin-A488 (1:100; Invitrogen). Secondary reagents included streptavidin (SA)-FluoProbe 547 (1:1500; Interchim, Montluçon, France), SA-Cy5 (1:1000; GE Healthcare Life Sciences, Chalfont St. Giles, UK), SA-A488 (1:400; Interchim), biotinylated rabbit anti-rat (1:200; Jackson ImmunoResearch Laboratories, West Grove, PA, USA), biotinylated goat anti-rabbit (1:200; Jackson ImmunoResearch Laboratories), and donkey anti-rabbit Cy3 (1:300; Jackson ImmunoResearch Laboratories). Sections were visualized using a fluorescence microscope (AxioImager Z1; Carl Zeiss). Image analysis was performed with Image Pro-Plus 6.3. Cardiac capillary density was quantified as the ratio of PECAM-1$^+$ vessels to the number of transversally sectioned cardiomyocytes per field. Endothelial proliferation was determined by counting Ki67 and PECAM-1 double-labeled cells. Proangiogenic M2-like macrophages were identified as F4/80$^+$ and CD206$^+$, whereas proinflammatory M1 macrophages were identified as F4/80$^+$ and CD206$^-$ cells. Cardiac CD45$^+$ and F4/80$^+$ cell infiltrations were calculated and reported as percent infiltration per field. The size of α-SMA$^+$ arteries was measured using the "draw object" tool in Image Pro-Plus 6.3.

Biochemistry

For the assessment of phospho-extracellular signal-regulated kinase (ERK) 1/2 and phospho-Akt, proteins were extracted in PhosphoSafe Extraction Reagent (Novagen, Madison, WI, USA) lysis buffer. Then 30 μg of protein/sample was separated by SDS-PAGE (Mini Gel Protean III System; Bio-Rad Laboratories, Hercules, CA, USA) and transferred to HyBond ECL membranes (Amersham Biosciences, Uppsala, Sweden) during 90 min at 100 V (Mini Trans-Blot Cell; Bio-Rad Laboratories). Membranes were incubated with either anti-phospho-ERK-1/2 (Cell Signaling Technology), anti-phospho-Akt (Cell Signaling Technology), or anti-glyceraldehyde-3-phosphate dehydrogenase (GAPDH; Sigma-Aldrich). Goat anti-rabbit or rabbit anti-goat horseradish peroxidase-conjugated secondary antibodies were used (Jackson ImmunoResearch Laboratories). Proteins were visualized with a chemiluminescence kit (Lumi-Light; Roche Molecular Biochemicals). Band densities were estimated using BioCapt and Bio-Profil software (BioID, Vilber Lourmat, France). Cardiac VEGF levels were quantified by enzyme-linked immunosorbent assay according to the manufacturer's instructions (R&D Systems).

For the quantification of VEGFR2, phosphorylated-Src/Src, and vascular endothelial cadherin (VE-cadherin), mice were anesthetized, 1 mM Na_3VO_4 and 2 mM H_2O_2 were injected into the tail vein, and the heart was dissected to remove the left ventricle, which was then snap-frozen. Proteins were extracted as described previously (14). In brief, after VEGFR2 immunoprecipitation, samples were analyzed by SDS-PAGE followed by Western blotting on nitrocellulose membranes. Anti-VEGFR2 (Cell Signaling Technology), anti-VE-cadherin (Santa Cruz Biotechnology), anti-Src kinase family (Cell Signaling Technology), and anti-phospho-Src family Tyr-416 (Cell Signaling Technology) antibodies were used. The signal was revealed by AttoPhos chemiluminescence (Promega), and band intensity was quantified by Quantity One 1-D Analysis Software (Bio-Rad Laboratories).

Magnetic resonance imaging (MRI)

Cardiac MRI was performed using a 4.7-T horizontal bore scanner (Bruker, Newark, DE, USA; refs. 1, 15) in mice anesthetized by intraperitoneal injection of 320 mg/kg chloral hydrate (Sigma-Aldrich). Cardiac perfusion was evaluated in the noninfarcted LV area by the arterial spin-labeling technique (1), in which the blood in the arteries upstream from the imaging volume is magnetically labeled. As a consequence, image intensity changes, depending on the blood supply to the tissue in the imaged slice. On subtraction of an image acquired without spin labeling, the background signal from static spins is removed, and the differential image can be used to quantify perfusion. The difference in the inverse of the apparent T1 images then yields a measure of the regional cardiac perfusion = $L\ (1/T1_{selective} - 1/T1_{nonselective})$, where L is the blood-tissue partition coefficient (16, 17).

LV function and hemodynamics

LV ejection fraction (percentage) and stroke volume were determined by MRI 3-dimensional reconstruction of the left ventricle (15).

LV hemodynamics were assessed using LV pressure-volume curves in mice anesthetized by intraperitoneal injection of 320 mg/kg chloral hydrate (Sigma-Aldrich). In brief, a 1.4-French miniaturized combined conductance catheter-micromanometer (model SPR-839; Millar Instruments Inc., Houston, TX, USA) connected to a pressure-conductance unit (MPCU-200; Millar Instruments) was advanced retrogradely *via* the carotid artery into the left ventricle. Pressure-volume loops were recorded at baseline and during loading by gently occluding the abdominal aorta with a cotton swab, allowing calculation of the LV end-systolic pressure-volume relation (LVESPVR) and LV end-diastolic pressure-volume relation (LVEDPVR) as indicators of load-independent LV passive elastance and compliance function, respectively (18).

Statistics

Data are presented as means ± SEM. Student's *t* test (2-tailed) was used to compare 2 groups of independent samples. For multiple comparisons, 1-way analysis of variance was used, followed by Tukey's *post hoc* test, except for immunoblotting of phosphorylated-Src/Src/VEGFR2 for which we used a nonparametric Mann-Whitney test. A value of $P < 0.05$ was considered significant.

RESULTS

Post-MI vascular remodeling is improved in PTP1B-deficient mice

To evaluate the effect of PTP1B deficiency on cardiac angiogenesis, we used the model of coronary artery ligation causing MI in *PTP1B*$^{-/-}$ and WT mice. Three months after MI, there was no difference in infarct size between groups (% left ventricle: WT, 39±1; *PTP1B*$^{-/-}$, 41±5%), indicating that the potential benefits in *PTP1B*$^{-/-}$ mice were not attributable to any change in this parameter (**Fig. 1*A***). A 22% increase in capillary density (capillaries/cardiomyocyte) was then measured in the whole left ventricle of *PTP1B*$^{-/-}$ infarcted mice compared with that in WT mice (Fig. 1*B*). Increased capillary density was also found when the value was expressed as capillaries/mm^2; however, this value was much smaller (+7%) and nonsignificant, most likely related to the increased myocyte size in both groups secondary to hypertrophy, which compensates for the massive loss of cardiac tissue in this context of very large infarcts.

Studying earlier time points, we also found increased angiogenesis at 8 d post-MI in the whole left ventricle of *PTP1B*$^{-/-}$ mice with an 18% increase in capillary density (Fig. 1*B*), whereas increased interstitial fibrosis was not yet histologically detectable (WT sham treatment, 2.8±0.3%; WT MI, 2.5±0.3%; and *PTP1B*$^{-/-}$ MI, 3.0±0.3; NS). Again, increased capillary density, but smaller (+6%) and nonsignificant, was also found when expressed as capillaries/mm^2. In addition, at 8 d, a significant stimulation of arteriogenesis was also detected in the infarct border zone of *PTP1B*$^{-/-}$ mice by counting the vessels coated with VSMCs, as shown by an increased number of small arteries (lumen diameter of 15–50 μm) without any change in the reduction in the density of small arterioles (lumen diameter of <15 μm; Fig. 1*E*).

At 3 d post-MI, with similar infarct sizes in both groups (% left ventricle: WT, 56±5% and *PTP1B*$^{-/-}$, 45±5%) showing no major difference in the healing process in progress (Fig. 1*A*), we found that in WT mice, MI was associated with a small decrease in capillary density (−8.1%) measured in the infarct border (Fig. 1*C*), which was absent in PTP1B-deficient mice (+7.2% *vs.* WT MI; $P = 0.05$). At this time point, we also detected increased endothelial cell proliferation (Ki67$^+$ nuclei/endothelial cells nuclei) in *PTP1B*$^{-/-}$ mice (Fig. 1*D*), which was absent at 8 d (data not shown).

Migration, apoptosis, and proliferation of cultured vascular cells is regulated by PTP1B

The effect on endothelial cell migration of PTP1B blockage or mRNA reduction was evaluated. Incubation of HMECs with the PTP1B inhibitor AS279 or transduction with specific shRNA resulting in a 60% decrease in PTP1B messengers in the HMEC Sh1 clone (Supplemental Fig. S1), led to increased spontaneous and increased VEGF-A-induced cell migration (**Fig. 2*A*, *B***). Comparable effects were observed with PDGF-BB in HMECs (Supplemental Fig. S2).

Apoptosis has been involved in the control of angiogenesis (19). *In vivo*, immunolabeling of cleaved caspase-3 was found as a rare event in mouse left ventricle at 3 d post-MI (data not shown) and a slightly higher apoptosis at 1 d post-MI showed no difference inside the ischemic area or at the border of or remote from the infarcted zone between *PTP1B*$^{-/-}$ and WT mice (Supplemental Fig. S3). However, *in vitro*, staurosporine-induced caspase-3 activity was decreased both in HMECs treated by AS279 and in the HMEC Sh1 clones (Fig. 2*C*), indicating reduced endothelial apoptosis.

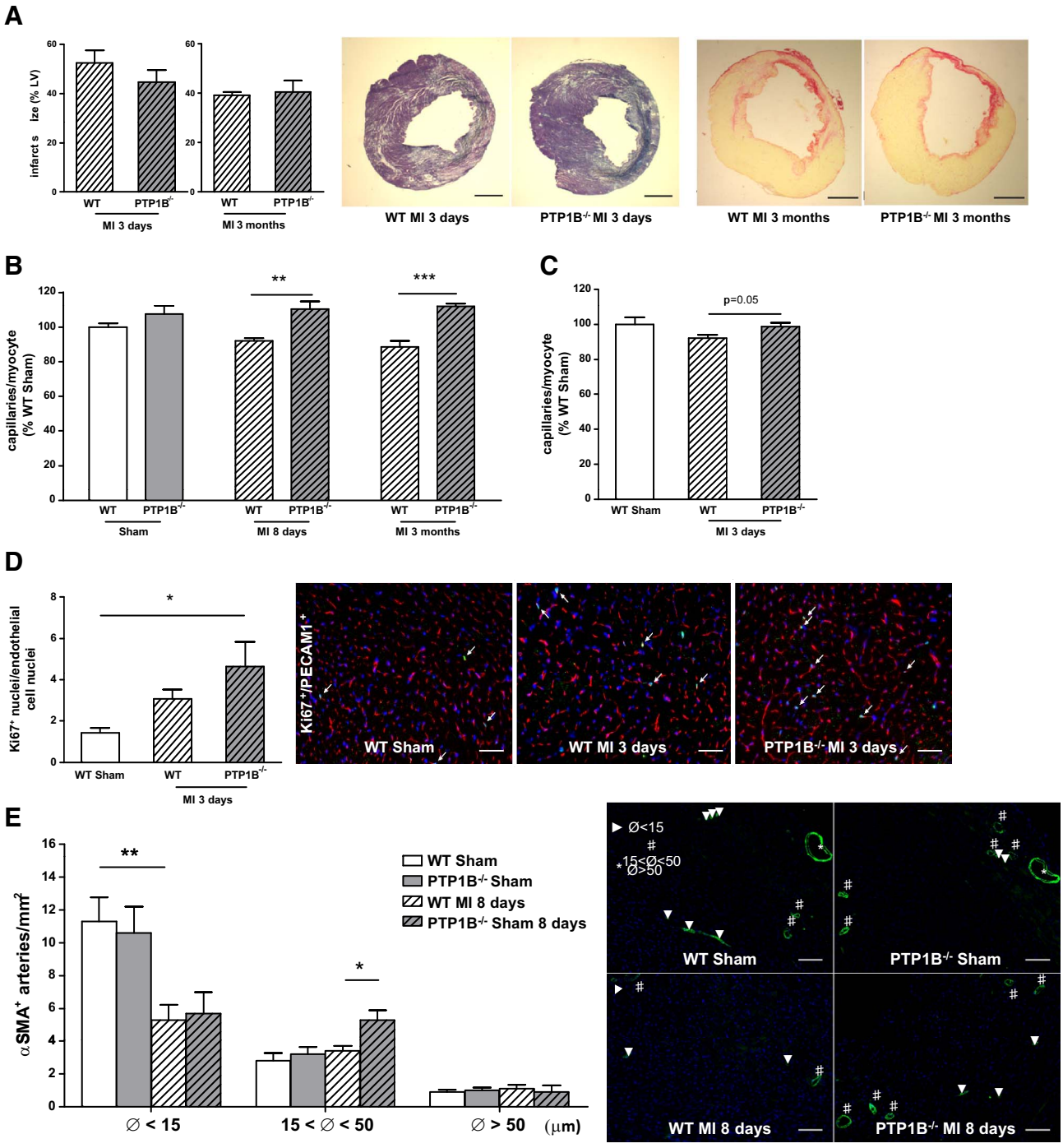

Figure 1. Post-MI vascular remodeling is improved in PTP1B-deficient mice. *A*) Infarct size quantification at 3 d (n=8) or 3 mo (n=5–10) post-MI and representative images of LV sections after Masson's trichrome staining (3 d post-MI) or sirius red staining (3 mo post-MI); ×1.25. Scale bars = 1 mm. *B*) LV capillaries/cardiomyocyte ratio (6 pictures/LV section, ×40, n=5–10/condition) assessed by PECAM-1 immunolabeled endothelial cells and wheat germ agglutinin staining for detection of cardiomyocyte sarcolemma at 8 d or 3 mo post-MI. *C*) LV capillaries/cardiomyocyte ratio at 3 d post-MI (n=6–9). *D*) Endothelial cell proliferation assessed by PECAM-1 and Ki67 double labeling (4 images/LV section; ×20; n=6–9); double-labeled cells are indicated with white arrows on representative images (PECAM-1 in red, Ki67 in green, and nuclei in blue; ×20). Scale bars = 50 μm. *E*) Density measurements of αSMA$^+$-labeled arteries according to vessel diameter at the infarct border zone 8 d after MI or in left ventricle of sham-treatd animals (minimum 4 pictures/LV section; ×10; n=5–7); lumen diameter of arteries (αSMA in green and nuclei in blue) is indicated (∅<15 μm, 15<∅<50 μm, and ∅>50 μm) on representative images (×10). Scale bars = 100 μm. *$P < 0.05$; **$P < 0.01$; ***$P < 0.001$.

Whether PTP1B inhibition influenced endothelial proliferation was also evaluated. Coincubation of VEGF-A with AS279, but not with VEGF-A alone, increased HMEC proliferation (Fig. 2*D*). Beyond endothelial cells, arteriogenesis requires the proliferation of VSMCs. Actually, PTP1B inhibition with

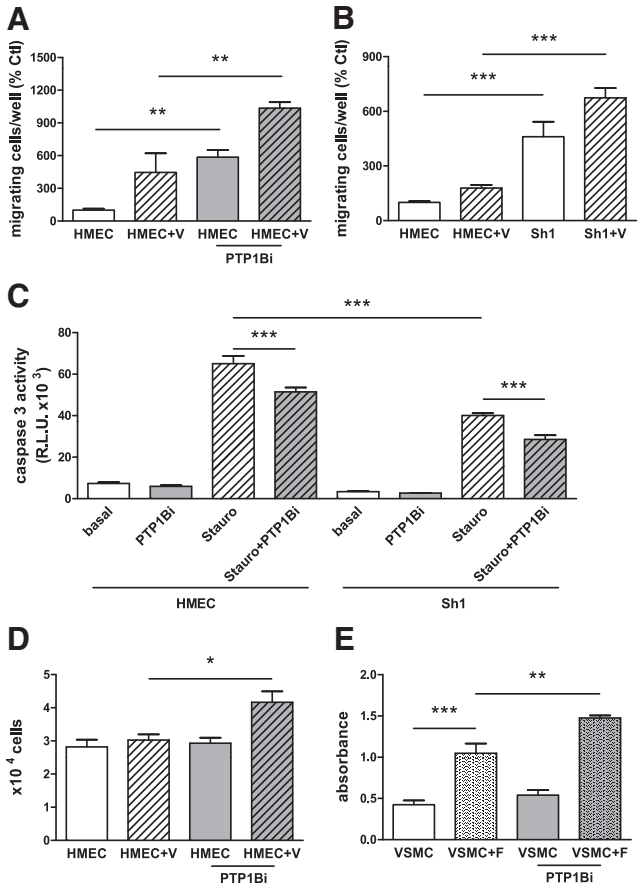

Figure 2. Enhanced migration, lowered apoptosis, and enhanced proliferation in cultured vascular cells treated by PTP1B antagonist or after PTP1B silencing using shRNA. *A*, *B*) Migration: HMECs (*A*, *B*) or HMEC Sh1 subclone expressing shRNA against PTP1B (*B*) were incubated in the presence or absence of 50 ng/ml VEGF-A (V) for 6 h, with or without PTP1B inhibitor 1 μM AS279 (PTP1Bi; $n=6$). *C*) Apoptosis: staurosporine treatment (+Stauro) was initiated in HMECs or HMEC Sh1 subclone with or without AS279 (PTP1Bi) before measurements of caspase-3 activity ($n=6$); R.L.U., relative luminescence units. *D*, *E*) Proliferation: HMECs (*D*) were incubated in the presence or absence of 25 ng/ml VEGF-A, with or without AS279 for 48 h, whereas rat aortic VSMCs in primary culture (*E*) were incubated in the presence or absence of 25 ng/ml FGF-2 (F), with or without AS279 (PTP1Bi) for 48 h ($n=4$). $*P < 0.05$; $**P < 0.01$; $***P < 0.001$.

AS279 enhanced FGF-2-induced proliferation in rat aortic VSMCs in primary culture (Fig. 2*E*).

Macrophage subsets analyzed at 3 d post-MI

Because immune cells are also implicated in myocardial healing, in part by secretion of growth factors involved in angiogenesis (20), we then analyzed macrophage subsets in response to MI in both genotypes. In the infarct border zone, there was no difference in the number of infiltrated immune cells ($CD45^+$ cells) or in the amount of monocytes/macrophages ($F4/80^+$ cells) between *PTP1B*$^{-/-}$ and WT mice (**Fig. 3**). However, 3 d after MI, *PTP1B*$^{-/-}$ mice displayed an increased number of proangiogenic M2-like macrophages ($CD206^+/F4/80^+$ cells, number of cells/field: WT sham treatment, 3±1; WT MI, 9±1; and *PTP1B*$^{-/-}$ MI, 14±1; $P<0.01$ *vs.* WT-MI), in contrast to proinflammatory M1 cells ($CD206^-/F4/80^+$ cells, number of cells/field: WT sham treatment, 8±2; WT MI, 25±4; and *PTP1B*$^{-/-}$ MI, 21±3; NS *vs.* WT MI; Fig. 3). Taken together, our data demonstrate a shift toward an increased proangiogenic anti-inflammatory activation state in macrophages of *PTP1B*$^{-/-}$ mice at 3 d post-MI compared with that for WT mice.

Signaling pathways involved in cardioprotection in PTP1B-deficient mice

The phosphatidylinositol 3-kinase (PI3K)/Akt signaling pathway is involved downstream of the insulin RTK, which was the first described to be targeted by PTP1B (3). We therefore performed Western blotting with the aim of investigating PI3K/Akt activation in LV samples from heart collected at 3 d post-MI. No alteration in the phosphorylation level of Akt was found in *PTP1B*$^{-/-}$ or WT mice. Because PTP1B also regulates VEGF signaling downstream of VEGFR2, we next sought to analyze ERK signaling in both genotypes. Increased phosphorylation of ERK2 kinase was seen 3 d after MI in *PTP1B*$^{-/-}$ mice compared with that in WT mice (**Fig. 4*A***).

Such quantifications of phosphorylated protein are related not only to endothelial cells but also to all cell types within the heart, primarily cardiomyocytes. To selectively investigate signaling pathways that operate in coronary vessels, the endothelial VEGFR2/VE-cadherin complex was further investigated. This complex is transiently dissociated in endothelial cells on MI as we demonstrated previously (14). Indeed, VEGFR2 activation leads to Src kinase phosphorylation, which in turn phosphorylates VE-cadherin, resulting in the dissociation of the complex (21). Immunoprecipitation of VEGFR2 showed an increased phosphorylated-Src/Src/VEGFR2 ratio, as well as increased dissociation of the VEGFR2/VE-cadherin complex in *PTP1B*$^{-/-}$ mice at 3 d post-MI (Fig. 4*B*). Notably, increased VEGFR2 activation in *PTP1B*$^{-/-}$ mice was not due to different VEGF-A levels, which were augmented equally at either 3 or 8 d post-MI in both *PTP1B*$^{-/-}$ and WT mice compared with those in sham-treated animals (Supplemental Fig. S4). Because VEGFR2 activation is involved not only in angiogenesis but also in vascular permeability, the occurrence of hemorrhage was investigated at 3 d post-MI and showed no difference between *PTP1B*$^{-/-}$ and WT mice (Supplemental Fig. S5).

Taken together, these results strongly support a mechanism by which increased activation of VEGFR2 signaling operates in coronary vessels from *PTP1B*$^{-/-}$ mice compared with that in WT mice, thereby contributing to efficient stimulation of vascular remodeling at early stages after MI.

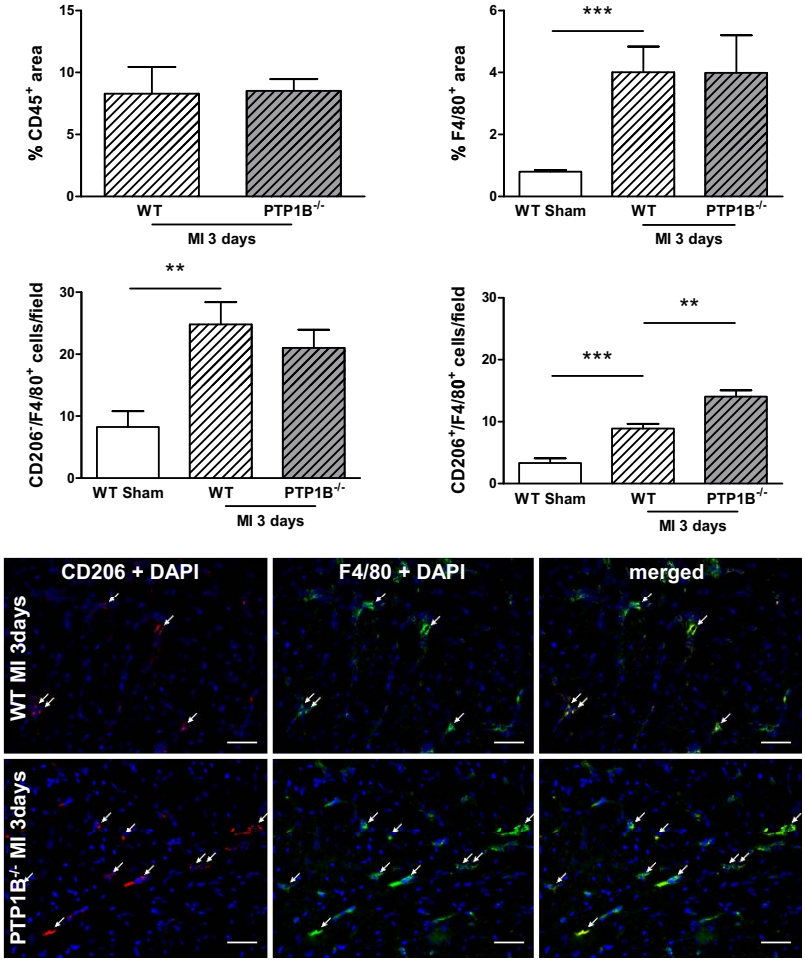

Figure 3. Increased numbers of proangiogenic anti-inflammatory macrophages at 3 d post-MI in PTP1B-deficient mice. Infiltrated cells (top left graph) and monocyte/macrophage recruitment (top right graph), respectively, assessed by CD45 and F4/80 immunolabeling (×10), reported as a percentage of field surface. Proinflammatory (bottom left graph) and proangiogenic (bottom right graph) macrophages assessed by double labeling of F4/80 and CD206 (×20) at the infarct border zone at 3 d post-MI or in the left ventricle of sham-treated animals, reported as mean number of macrophages per field (4 images/mouse; n=6–9). Increased numbers of proangiogenic anti-inflammatory macrophages (indicated with white arrows) in *PTP1B*$^{-/-}$ mice at 3 d post-MI are illustrated on representative images (CD206 in red, F4/80 in green, and nuclei in blue; ×20). Scale bars = 50 μm. DAPI, 4′,6′-diamidino-2-phenylindole. $^{**}P < 0.01$; $^{***}P < 0.001$.

LV perfusion and LV function are improved at 8 d post-MI in PTP1B-deficient mice

To determine how increased activation of VEGFR2 signaling and angiogenesis translate into functional activity of the heart, the perfusion levels in the noninfarcted area of the left ventricle were then measured using MRI. Before MI, there was no difference in myocardial perfusion between WT and *PTP1B*$^{-/-}$ mice (**Fig. 5*A***). In contrast, at 8 d post-MI, the myocardial perfusion was significantly higher in *PTP1B*$^{-/-}$ mice than in WT mice (Fig. 5*A*).

At 8 d post-MI, MRI analysis did not yet show any advantages of PTP1B deficiency with respect to ejection fraction and stroke volume, which were similarly decreased in all infarcted animals regardless of the genotype (Fig. 5*B*). The early analyses of LV function by invasive pressure-volume loops at this time point showed decreased LVESPVR, indicating reduced elastance and occurrence of systolic dysfunction, which was not modified by PTP1B deficiency. In contrast and remarkably, the benefits on diastolic function were detectable in infarcted *PTP1B*$^{-/-}$ mice. Indeed, although LVEDPVR was increased in WT MI mice, it was not increased in *PTP1B*$^{-/-}$ MI mice, clearly illustrating better compliance and reduced diastolic dysfunction (Fig. 5*C*).

These results suggest that improved myocardial perfusion, which takes place in diastole, contributed to early improvement in post-MI diastolic function in *PTP1B*$^{-/-}$ mice *via* an improvement in LV compliance.

DISCUSSION

The main result of this study is that *PTP1B* gene invalidation improves both angiogenesis and arteriogenesis after MI, leading to improved cardiac perfusion that most likely contributes to the early protection against diastolic dysfunction. These events represent the original cardiac benefits explaining long-term reduction in heart failure induced by PTP1B deficiency that we reported previously (10).

Murine HMECs (11) were used as a model to assess angiogenic processes, particularly in microvascular cardiac endothelial cells. A PTP1B inhibitor or shRNA diminished staurosporine-induced activation of caspase-3 in HMECs, indicating *in vitro* reduced apoptosis as shown previously in fibroblasts, hepatocytes, and cardiomyocytes (22–24). This effect was not found in the myocardium of *PTP1B*$^{-/-}$ compared to WT mice 24 h after coronary artery ligation. Nevertheless, the low frequency of apoptosis at this time point rendered comparative quantification difficult.

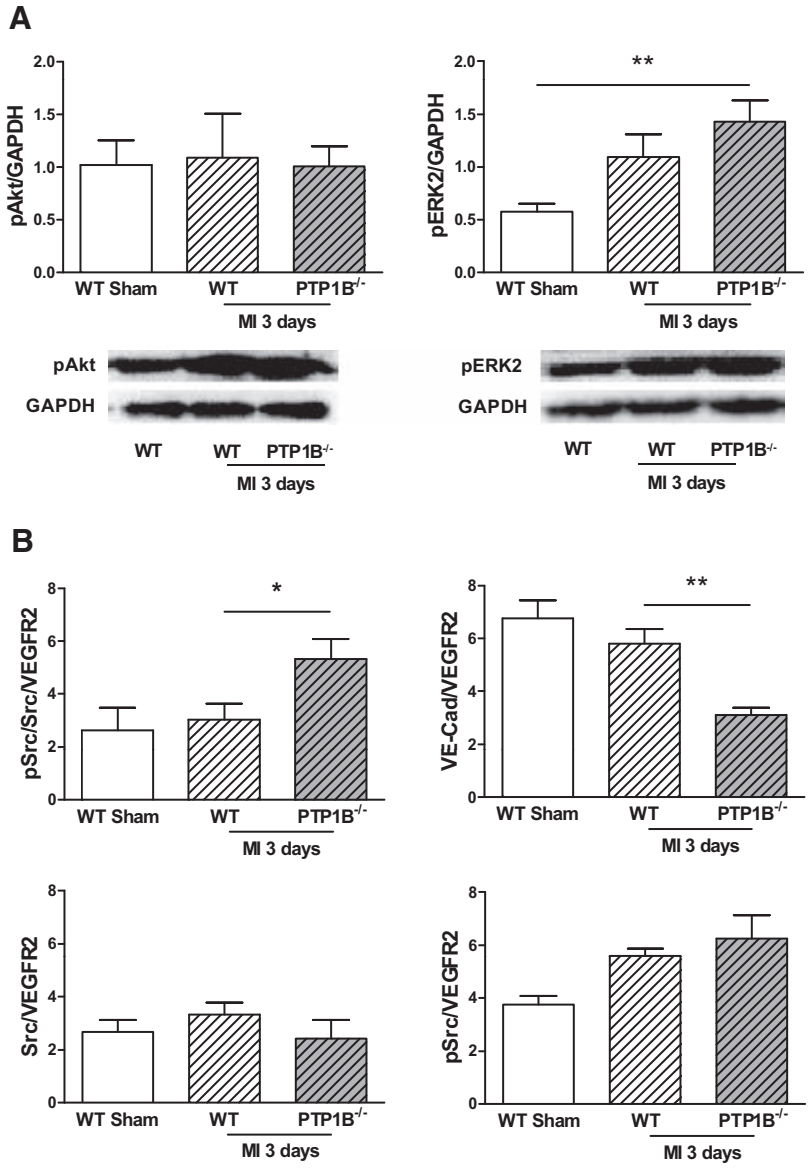

Figure 4. Enhanced VEGFR2 activation at 3 d post-MI in PTP1B-deficient mice. *A*) Phospho-Akt and phospho-ERK-2 levels normalized to GAPDH (n=5–10). *B*) Immunoprecipitation of VEGFR2 showed an increased phosphorylated-Src/Src/VEGFR2 ratio, as well as increased dissociation of the VEGFR2/VE-cadherin complex, in *PTP1B*$^{-/-}$ mice at 3 d post-MI. VE-cadherin (VE-Cad), Src kinase (Src), phospho-Src kinase (pSrc), and phospho-Src kinase on Src kinase levels normalized to immunoprecipitated VEGFR2 (n=6). *$P < 0.05$; **$P < 0.01$.

Notably, decreasing PTP1B expression and/or activity increased spontaneous and VEGF-induced HMEC migration. The boosted migration in the absence of VEGF may be explained by a destabilization of endothelial cell adherens junctions mediated by increased activation of VE-cadherin. Indeed, experiments performed in human umbilical vein endothelial cells (HUVECs) showed that PTP1B interacts with VE-cadherin, so that PTP1B down-regulation leads to increased VE-cadherin phosphorylation, inducing destabilization of endothelial cell-cell junctions (5), which constitutes a necessary initial step during endothelial cell migration. Another explanation is activation of RTKs independent of ligand binding (25). Indeed, PTP1B, which is either anchored in the endoplasmic reticulum or directed to the plasma membrane, can dephosphorylate growth factor receptors when they are being synthesized in the endoplasmic reticulum (26).

Beyond the capillaries, coordinated endothelial proliferation/migration followed by coverage of neovessels by VSMCs is necessary for the maturation of blood vessels. In our hands, PTP1B inhibition increased FGF-induced proliferation of primary rat VSMCs. This result is consistent with results of a previous study from another group showing that overexpression of native or dominant-negative PTP1B in cultured VSMCs, respectively, blocked or enhanced FGF-induced migration (7). However, to our knowledge, this is the first time that PTP1B deficiency reflects an ability to stimulate *in vivo* arteriogenesis, at least under cardiac pathophysiological conditions. Indeed, the arteriolar rarefaction induced by MI was thwarted in *PTP1B*-deficient mice, as a result of increased density of small arteries (diameter of 15–50 μm) as soon as 8 d after ischemia. Nevertheless, the increased number of arteries assessed histologically might have reflected nonfunctional blood vessels, for example, arteries with severe endothelial dysfunction and/or altered vasomotor function. MRI analysis at 8 d post-MI showed normalized myocardial perfusion in the viable part of the left ventricle of *PTP1B*$^{-/-}$ mice, confirming the functionality of these blood vessels.

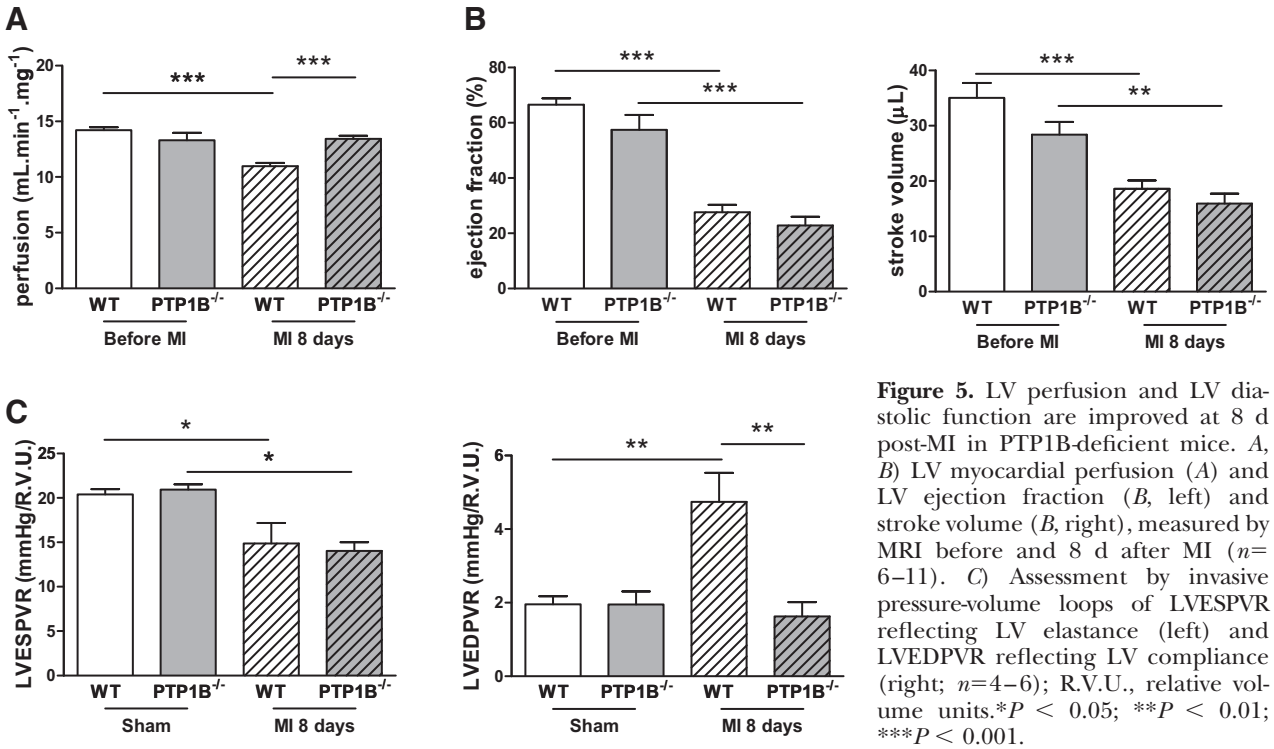

Figure 5. LV perfusion and LV diastolic function are improved at 8 d post-MI in PTP1B-deficient mice. *A*, *B*) LV myocardial perfusion (*A*) and LV ejection fraction (*B*, left) and stroke volume (*B*, right), measured by MRI before and 8 d after MI (n=6–11). *C*) Assessment by invasive pressure-volume loops of LVESPVR reflecting LV elastance (left) and LVEDPVR reflecting LV compliance (right; n=4–6); R.V.U., relative volume units.*$P < 0.05$; **$P < 0.01$; ***$P < 0.001$.

Analysis of the effect of PTP1B deficiency in normal mice (no infarct) revealed no detectable changes on the various parameters of angiogenesis/arteriogenesis or myocardial perfusion. This finding may reflect a minor role of this enzyme in the regulation of the response to angiogenic growth factors in adults in the absence of an increased angiogenic stimulus, suggesting that activity of this enzyme becomes limiting only in situations of active angiogenesis (such as that occurring in the presence of hypoxia or ischemia) or that PTP1B gene deficiency is compensated for by expression of other phosphatases (27).

Molecular studies at 3 d post-MI implied VEGFR2 activation in the proangiogenic effects of PTP1B deficiency *via* increased phosphorylation of Src kinase at tyrosine Y416 and subsequently increased VEGFR2/VE-cadherin dissociation. These *in vivo* findings support a study in cultured HUVECs in which an siRNA against PTP1B allowed increased VEGF-induced VEGFR2 phosphorylation, whereas PTP1B overexpression reduced it (5). A mechanism by which PTP1B acts on VEGFR2 was proposed in a study of femoral artery ligation in synectin-deficient mice presenting altered arteriogenesis (28). The absence of synectin in endothelial cells induced a delay in VEGFR2 endocytosis and a decrease in its activation, which was explained by prolonged contact with PTP1B at the plasma membrane. Indeed, pharmacological inhibition of PTP1B restored arterial morphogenesis in synectin-deficient mice. Moreover, VEGF binding to VEGFR2 induces the activation of Src kinase in a T cell-specific adapter-dependent manner, allowing increased Src phosphorylation at Y416 and reduced phosphorylation at Y527 (29). PTP1B was described as an activator of Src by dephosphorylating pY527 (30). However, the absence of functional PTP1B did not impede the overall activation of Src at 3 d post-MI, resulting in increased dissociation of the VEGFR2/VE-cadherin complex.

Concerning the infiltrate during ischemia, 2 monocyte/macrophage populations have been described: the classic M1 type, which is proinflammatory and participates in the very early infarct healing phase by engulfing necrotic cardiomyocytes, and the M2-like type, which promotes angiogenesis *via* release of growth factors (31, 32). We found a higher infiltration of proangiogenic M2-type macrophages, characterized by F4/80-CD206 double-positive labeling (33) in the infarct border zone of *PTP1B*$^{-/-}$ mice at 3 d post-MI, with no difference in total macrophage infiltration. Thus, although the direct link has not been fully demonstrated, it is possible that this increased M2 infiltration contributes to the stimulated angiogenesis in *PTP1B*$^{-/-}$ mice with MI.

One of the mechanisms explaining the increased angiogenesis observed in *PTP1B*$^{-/-}$ mice may involve endothelial nitric oxide (NO). We previously reported that PTP1B inhibition or gene invalidation protected from endothelial dysfunction 2 mo after MI, in particular through maintained production of NO secondary to increased activation of endothelial NO synthase (eNOS; refs. 10, 12). In the context of angiogenesis, an increase in endothelial NO participates in the destabilization of the endothelial cell junction together with the vasodilation that precedes sprouting (34), whereas decreased NO release and endothelial dysfunction have a negative affect on angiogenesis (35). However, the NO donor *S*-nitroso-*N*-acetyl-DL-penicillamine (SNAP) has been reported to reduce motility of cultured aortic

VSMCs by lowering the phosphorylation level of adhesion proteins such as paxillin or focal adhesion kinase, in direct relation to increased PTP1B activity (9, 36). This apparent paradoxical opposite effect of the endothelial *vs.* VSMC PTP1B/NO pathways may be explained in part by the known concentration dependence of the effects of NO, because in those studies SNAP was shown to exert its effects at concentrations between 1 and 100 μM, whereas eNOS presumably produces NO at much lower concentrations.

Concerning functional data, we observed improved LV diastolic function at 8 d post-MI. No direct link has been described between enhancement of angiogenesis and early improvement of diastolic function after MI, although it is likely that increased myocardial perfusion may contribute to preservation of diastolic function. Furthermore, there is evidence that impaired NO production worsens diastolic function, whereas, conversely, stimulation of NO production or administration of NO-releasing molecules improves it (18, 37). Thus, it is possible that the improved diastolic function may benefit from enhanced angiogenesis and perfusion in combination with the endothelial protective effects of PTP1B deficiency.

The improved diastolic function at 8 d occurred with no evidence of improved systolic function at this early time point. We previously reported, in a completely different set of experiments but using the same model, increased LV function at 1 and 2 mo post-MI, evidenced by improved echocardiographic parameters of LV remodeling and function, as well as improved LV hemodynamics and decreased fibrosis at 2 mo (10). Because of this report, we did not repeat a similar functional analysis at a time point later than 8 d in the present study; however, taken together, the results of this previous study and the present study suggest a time course of functional recovery in *PTP1B*$^{-/-}$ mice first involving improved diastolic function followed later by improved systolic and diastolic function and reduced adverse LV remodeling.

A recent study from our laboratory showed that selective angiogenic/arteriogenic therapy by intramyocardial sustained delivery of a growth factor combination including FGF and HGF prevents CHF in a rat MI model (1), demonstrating the direct role of angiogenesis/arteriogenesis stimulation in the reduction of heart failure. Thus, although other mechanisms such as prevention of endothelial dysfunction and increased insulin signaling may play a role, it is likely that the improved early post-MI angiogenesis/arteriogenesis revealed in the present study contributes to the overall reduction of CHF observed in our previous work at 1 and 2 mo post-MI (10).

CONCLUSIONS

The results presented here suggest for the first time that blocking of PTP1B may be a target for improving angiogenesis after myocardial infarction, ultimately resulting in reduced cardiac remodeling and dysfunction during heart failure. FJ

The authors thank Dr. Sébastien Banquet, Dr. Manuelle Debunne, and Inès Boukhalfa for valuable help; Dr. Michel L. Tremblay (Goodman Cancer Centre, McGill University, Montreal, QC, Canada) for providing the PTP1B-deficient mice; and Brigitte Dautréaux, Sylvanie Renet, and Laetitia Guedin for their excellent technical assistance. The study was supported in part by a grant from the Fondation de France. M.B. and A.G. are recipients of a Ph.D. grant from the French Ministry of Research and Education, and D.C. is a recipient of a Ph.D. grant from the Région Haute Normandie. The authors declare no conflicts of interest.

REFERENCES

1. Banquet, S., Gomez, E., Nicol, L., Edwards-Levy, F., Henry, J. P., Cao, R., Schapman, D., Dautreaux, B., Lallemand, F., Bauer, F., Cao, Y., Thuillez, C., Mulder, P., Richard, V., and Brakenhielm, E. (2011) Arteriogenic therapy by intramyocardial sustained delivery of a novel growth factor combination prevents chronic heart failure. *Circulation* **124,** 1059–1069
2. Carmeliet, P. (2005) Angiogenesis in life, disease and medicine. *Nature* **438,** 932–936
3. Elchebly, M., Payette, P., Michaliszyn, E., Cromlish, W., Collins, S., Loy, A. L., Normandin, D., Cheng, A., Himms-Hagen, J., Chan, C. C., Ramachandran, C., Gresser, M. J., Tremblay, M. L., and Kennedy, B. P. (1999) Increased insulin sensitivity and obesity resistance in mice lacking the protein tyrosine phosphatase-1B gene. *Science* **283,** 1544–1548
4. Cheng, A., Uetani, N., Simoncic, P. D., Chaubey, V. P., Lee-Loy, A., McGlade, C. J., Kennedy, B. P., and Tremblay, M. L. (2002) Attenuation of leptin action and regulation of obesity by protein tyrosine phosphatase 1B. *Dev. Cell* **2,** 497–503
5. Nakamura, Y., Patrushev, N., Inomata, H., Mehta, D., Urao, N., Kim, H. W., Razvi, M., Kini, V., Mahadev, K., Goldstein, B. J., McKinney, R., Fukai, T., and Ushio-Fukai, M. (2008) Role of protein tyrosine phosphatase 1B in vascular endothelial growth factor signaling and cell-cell adhesions in endothelial cells. *Circ. Res.* **102,** 1182–1191
6. Markova, B., Herrlich, P., Ronnstrand, L., and Bohmer, F. D. (2003) Identification of protein tyrosine phosphatases associating with the PDGF receptor. *Biochemistry* **42,** 2691–2699
7. Chang, Y., Ceacareanu, B., Zhuang, D., Zhang, C., Pu, Q., Ceacareanu, A. C., and Hassid, A. (2006) Counter-regulatory function of protein tyrosine phosphatase 1B in platelet-derived growth factor- or fibroblast growth factor-induced motility and proliferation of cultured smooth muscle cells and in neointima formation. *Arterioscler. Thromb. Vasc. Biol.* **26,** 501–507
8. Kakazu, A., Sharma, G., and Bazan, H. E. (2008) Association of protein tyrosine phosphatases (PTPs)-1B with c-Met receptor and modulation of corneal epithelial wound healing. *Invest. Ophthalmol. Vis. Sci.* **49,** 2927–2935
9. Hassid, A., Huang, S., and Yao, J. (1999) Role of PTP-1B in aortic smooth muscle cell motility and tyrosine phosphorylation of focal adhesion proteins. *Am. J. Physiol.* **277,** H192–H198
10. Gomez, E., Vercauteren, M., Kurtz, B., Ouvrard-Pascaud, A., Mulder, P., Henry, J. P., Besnier, M., Waget, A., Hooft Van Huijsduijnen, R., Tremblay, M. L., Burcelin, R., Thuillez, C., and Richard, V. (2012) Reduction of heart failure by pharmacological inhibition or gene deletion of protein tyrosine phosphatase 1B. *J. Mol. Cell. Cardiol.* **52,** 1257–1264
11. Gumkowski, F., Kaminska, G., Kaminski, M., Morrissey, L. W., and Auerbach, R. (1987) Heterogeneity of mouse vascular endothelium. In vitro studies of lymphatic, large blood vessel and microvascular endothelial cells. *Blood Vessels* **24,** 11–23
12. Vercauteren, M., Remy, E., Devaux, C., Dautreaux, B., Henry, J. P., Bauer, F., Mulder, P., Hooft van Huijsduijnen, R., Bombrun, A., Thuillez, C., and Richard, V. (2006) Improvement of peripheral endothelial dysfunction by protein tyrosine phosphatase inhibitors in heart failure. *Circulation* **114,** 2498–2507

13. Mulder, P., Barbier, S., Chagraoui, A., Richard, V., Henry, J. P., Lallemand, F., Renet, S., Lerebours, G., Mahlberg-Gaudin, F., and Thuillez, C. (2004) Long-term heart rate reduction induced by the selective I_f current inhibitor ivabradine improves left ventricular function and intrinsic myocardial structure in congestive heart failure. *Circulation* **109,** 1674–1679
14. Galaup, A., Gomez, E., Souktani, R., Durand, M., Cazes, A., Monnot, C., Teillon, J., Le Jan, S., Bouleti, C., Briois, G., Philippe, J., Pons, S., Martin, V., Assaly, R., Bonnin, P., Ratajczak, P., Janin, A., Thurston, G., Valenzuela, D. M., Murphy, A. J., Yancopoulos, G. D., Tissier, R., Berdeaux, A., Ghaleb, B., and Germain, S. (2011) Protection against myocardial infarction and no-reflow through preservation of vascular integrity by angiopoietin-like 4. *Circulation* **125,** 140–149
15. Merabet, N., Bellien, J., Glevarec, E., Nicol, L., Lucas, D., Remy-Jouet, I., Bounoure, F., Dreano, Y., Wecker, D., Thuillez, C., and Mulder, P. (2011) Soluble epoxide hydrolase inhibition improves myocardial perfusion and function in experimental heart failure. *J. Mol. Cell. Cardiol.* **52,** 660–666
16. Bauer, W. R., Hiller, K. H., Roder, F., Rommel, E., Ertl, G., and Haase, A. (1996) Magnetization exchange in capillaries by microcirculation affects diffusion-controlled spin-relaxation: a model which describes the effect of perfusion on relaxation enhancement by intravascular contrast agents. *Magn. Reson. Med.* **35,** 43–55
17. Kober, F., Iltis, I., Izquierdo, M., Desrois, M., Ibarrola, D., Cozzone, P. J., and Bernard, M. (2004) High-resolution myocardial perfusion mapping in small animals in vivo by spin-labeling gradient-echo imaging. *Magn. Reson. Med.* **51,** 62–67
18. Fang, Y., Nicol, L., Harouki, N., Monteil, C., Wecker, D., Debunne, M., Bauer, F., Lallemand, F., Richard, V., Thuillez, C., and Mulder, P. (2011) Improvement of left ventricular diastolic function induced by β-blockade: a comparison between nebivolol and metoprolol. *J. Mol. Cell. Cardiol.* **51,** 168–176
19. Dimmeler, S., and Zeiher, A. M. (2000) Endothelial cell apoptosis in angiogenesis and vessel regression. *Circ. Res.* **87,** 434–439
20. Nahrendorf, M., and Swirski, F. K. (2013) Monocyte and macrophage heterogeneity in the heart. *Circ. Res.* **112,** 1624–1633
21. Weis, S., Shintani, S., Weber, A., Kirchmair, R., Wood, M., Cravens, A., McSharry, H., Iwakura, A., Yoon, Y. S., Himes, N., Burstein, D., Doukas, J., Soll, R., Losordo, D., and Cheresh, D. (2004) Src blockade stabilizes a Flk/cadherin complex, reducing edema and tissue injury following myocardial infarction. *J. Clin. Invest.* **113,** 885–894
22. Buckley, D. A., Cheng, A., Kiely, P. A., Tremblay, M. L., and O'Connor, R. (2002) Regulation of insulin-like growth factor type I (IGF-I) receptor kinase activity by protein tyrosine phosphatase 1B (PTP-1B) and enhanced IGF-I-mediated suppression of apoptosis and motility in PTP-1B-deficient fibroblasts. *Mol. Cell. Biol.* **22,** 1998–2010
23. Gonzalez-Rodriguez, A., Escribano, O., Alba, J., Rondinone, C. M., Benito, M., and Valverde, A. M. (2007) Levels of protein tyrosine phosphatase 1B determine susceptibility to apoptosis in serum-deprived hepatocytes. *J. Cell Physiol.* **212,** 76–88
24. Song, H., Zhang, Z., and Wang, L. (2008) Small interference RNA against PTP-1B reduces hypoxia/reoxygenation induced apoptosis of rat cardiomyocytes. *Apoptosis* **13,** 383–393
25. Lammers, R., Bossenmaier, B., Cool, D. E., Tonks, N. K., Schlessinger, J., Fischer, E. H., and Ullrich, A. (1993) Differential activities of protein tyrosine phosphatases in intact cells. *J. Biol. Chem.* **268,** 22456–22462
26. Stuible, M., and Tremblay, M. L. (2010) In control at the ER: PTP1B and the down-regulation of RTKs by dephosphorylation and endocytosis. *Trends Cell Biol.* **20,** 672–679
27. Haj, F.G., Markova, B., Klaman, L.D., Bohmer, F.D. and Neel, B.G. (2003) Regulation of receptor tyrosine kinase signaling by protein tyrosine phosphatase-1B. *J. Biol. Chem.* **278,** 739–744.
28. Lanahan, A. A., Hermans, K., Claes, F., Kerley-Hamilton, J. S., Zhuang, Z. W., Giordano, F. J., Carmeliet, P., and Simons, M. (2010) VEGF receptor 2 endocytic trafficking regulates arterial morphogenesis. *Dev. Cell* **18,** 713–724
29. Sun, Z., Li, X., Massena, S., Kutschera, S., Padhan, N., Gualandi, L., Sundvold-Gjerstad, V., Gustafsson, K., Choy, W. W., Zang, G., Quach, M., Jansson, L., Phillipson, M., Abid, M. R., Spurkland, A., and Claesson-Welsh, L. (2012) VEGFR2 induces c-Src signaling and vascular permeability in vivo via the adaptor protein TSAd. *J. Exp. Med.* **209,** 1363–1377
30. Hebert Chatelain, E., Dupuy, J. W., Letellier, T., and Dachary-Prigent, J. (2010) Functional impact of PTP1B-mediated Src regulation on oxidative phosphorylation in rat brain mitochondria. *Cell. Mol. Life Sci.* **68,** 2603–2613
31. Nahrendorf, M., Swirski, F. K., Aikawa, E., Stangenberg, L., Wurdinger, T., Figueiredo, J. L., Libby, P., Weissleder, R., and Pittet, M. J. (2007) The healing myocardium sequentially mobilizes two monocyte subsets with divergent and complementary functions. *J. Exp. Med.* **204,** 3037–3047
32. Brechot, N., Gomez, E., Bignon, M., Khallou-Laschet, J., Dussiot, M., Cazes, A., Alanio-Brechot, C., Durand, M., Philippe, J., Silvestre, J. S., Van Rooijen, N., Corvol, P., Nicoletti, A., Chazaud, B., and Germain, S. (2008) Modulation of macrophage activation state protects tissue from necrosis during critical limb ischemia in thrombospondin-1-deficient mice. *PLoS One* **3,** e3950
33. He, H., Xu, J., Warren, C. M., Duan, D., Li, X., Wu, L., and Iruela-Arispe, M. L. (2012) Endothelial cells provide an instructive niche for the differentiation and functional polarization of M2-like macrophages. *Blood* **120,** 3152–3162
34. Dvorak, H. F., Brown, L. F., Detmar, M., and Dvorak, A. M. (1995) Vascular permeability factor/vascular endothelial growth factor, microvascular hyperpermeability, and angiogenesis. *Am. J. Pathol.* **146,** 1029–1039
35. Yu, J., deMuinck, E. D., Zhuang, Z., Drinane, M., Kauser, K., Rubanyi, G. M., Qian, H. S., Murata, T., Escalante, B., and Sessa, W. C. (2005) Endothelial nitric oxide synthase is critical for ischemic remodeling, mural cell recruitment, and blood flow reserve. *Proc. Natl. Acad. Sci. U.S.A.* **102,** 10999–11004
36. Hassid, A., Yao, J., and Huang, S. (1999) NO alters cell shape and motility in aortic smooth muscle cells via protein tyrosine phosphatase 1B activation. *Am. J. Physiol.* **277,** H1014–H1026
37. Westermann, D., Riad, A., Richter, U., Jager, S., Savvatis, K., Schuchardt, M., Bergmann, N., Tolle, M., Nagorsen, D., Gotthardt, M., Schultheiss, H. P., and Tschope, C. (2009) Enhancement of the endothelial NO synthase attenuates experimental diastolic heart failure. *Basic Res. Cardiol.* **104,** 499–509

Received for publication December 30, 2013.
Accepted for publication April 7, 2014.